

**Pressure-induced structural phase transition in Li₄Ge**

Journal:	<i>CrystEngComm</i>
Manuscript ID	CE-COM-05-2018-000783.R2
Article Type:	Communication
Date Submitted by the Author:	17-Aug-2018
Complete List of Authors:	Hao, Chunmei; Jiangsu Normal University Li, Yunguo; Royal Institute of Technology (KTH), Department of Materials and Engineering; University College London, Zhu, Qiang; Stony Brook University, Geosciences Chen, Xinxi; Jiangsu Normal University, School of Physics and Electronic Engineering, Wang, Zhanxin ; Jiangsu Normal University, School of Physics and Electronic Engineering, Li, Yan-ling; Jiangsu Normal University, School of Physics and Electronic Engineering,

Pressure-induced structural phase transition in Li_4Ge

Chun-Mei Hao¹, Yunguo Li¹, Qiang Zhu^{2,*}, Xin-Yi Chen¹, Zhan-Xin Wang¹, and Yan-Ling Li^{1,*}

1. School of Physics and Electronic Engineering, Jiangsu Normal University, Xuzhou 221116, China

2. Department of Physics and astronomy, University of Nevada Las Vegas, Las Vegas, NV, 89154-4002, USA

Abstract

The structural, dynamical, elastic, and electronic properties of Li_4Ge were investigated by the means of evolutionary crystal structure prediction in conjunction with first-principles calculations. We find that the ground-state Li_4Ge at ambient conditions has a cubic symmetry. Li_4Ge undergoes a structural phase transition at about 2 GPa from the cubic $P2_13$ phase to the $R-3m$ phase. The dynamical and mechanical stabilities of $P2_13$ and $R-3m$ were confirmed by the phonon and elastic constants calculations. From the calculated elastic constants, we obtained the elastic moduli and discussed its elastic anisotropy effect. Our calculation shows that the $P2_13$ structure is brittle while the $R-3m$ structure is ductile. The anisotropic property of $R-3m$ is more pronounced than $P2_13$ at ambient pressure. $P2_13\text{-Li}_4\text{Ge}$ is a narrow band gap semiconductor while $R-3m$ phase a poor metal.

1. Introduction

Clean energy has attracted extensive attention in recent years because of the increasing pressure from nonrenewable resource depletion and environmental pollution. Unfortunately, most clean energy sources like the solar energy, wind energy, and tidal energy, are intermittent and not convenient for direct utilization. Therefore, rechargeable energy storage devices are pivotal components in the clean energy conversion–storage–usage chain to realize their stable and efficient use.^{1,2} Lithium-ion batteries (LIBs) as the new next-generation batteries just satisfy the demand for the advanced portable electronic devices, electric vehicles, and large-scale energy storage. In search of new anode materials for LIBs, much attention has been paid to the potential application of group IV elements (Si, Ge, Sn) in compound forms.³ Compared with silicon and tin, the expensive germanium draws less attention. However, the diffusivity of lithium ion (about 400 times) and electronic conductivity (about 10^4 times) in germanium-based materials are greater than that in silicon. Besides, germanium-based batteries on low operating voltage have remarkable mechanical strength and theoretical capacity of 1600 mAh/g, about five times greater than tin (990 mAh/g).^{4,5,6} In addition, Ge electrodes react with Li through a reversible formation of a nanoporous network, permitting a facile stress relaxation, whereas Si electrodes are often heavily fractured.⁷ Germanium has also been proposed as a protective coating for SiNW anodes.^{8,9} These observations showing advantages of germanium-based batteries prompt further studies on the Li-Ge system.

To understand the discharge/charge process and improve the performance of Li-Ge batteries, many researches have been done on Li-Ge binary compounds. Sangster *et al*¹⁰ reported a binary phase diagram of the Li–Ge system consisting of seven experimentally reported crystalline phases: $\text{Li}_7\text{Ge}_{12}$, LiGe , $\text{Li}_{11}\text{Ge}_6$, Li_9Ge_4 , Li_7Ge_2 , $\text{Li}_{15}\text{Ge}_4$, and $\text{Li}_{22}\text{Ge}_5$. It is worth noting that the $\text{Li}_{22}\text{Ge}_5$ phase has been reformulated

as $\text{Li}_{17}\text{Ge}_4$ in 2001.¹¹ With the development of technology and ongoing research, new structures were successively reported. Some new Li-Ge compounds (Li_5Ge_2 , $\text{Li}_{13}\text{Ge}_5$, Li_8Ge_3 and $\text{Li}_{13}\text{Ge}_4$) were found via the combined random structure searching and atomic species swapping methods.¹² Jung *et al.*¹³ proved that during the discharge process, crystalline Ge first reacts to form a mixture of amorphous and crystalline Li_7Ge_3 which was proposed to be stable in the theoretical study of Morris *et al.*¹² Surprisingly, although Li_4Ge ¹³⁻¹⁷ has been suggested for many years in experiment and some researches on stoichiometries around 4:1 ($\text{Li}_{4.4}\text{Ge}$ ^{12,18,19,20}, $\text{Li}_{4.2}\text{Ge}$ ²¹, $\text{Li}_{4.10}\text{Ge}$ ²², $\text{Li}_{4.25}\text{Ge}$ ²²) have been reported, the structural information and corresponding properties of Li_4Ge have not yet been determined so far. Given that the analogical compounds Li_4Si ²³, Li_4Sn ²⁴ and K_4Si ²⁵, and Li_4C ²⁶ have been reported, it is highly likely that Li_4Ge may exist as well. This motivated us to explore the stable structure and physical properties of Li_4Ge in the present work.

We have systematically investigated the crystal structures of Li_4Ge up to 10 GPa. Firstly, two competing phases ($P2_13\text{-Li}_4\text{Ge}$ and $R\text{-}3m\text{-Li}_4\text{Ge}$) have been identified with the help of the evolutionary crystal structure prediction as implemented in the USPEX code.²⁷⁻²⁹ The dynamic stabilities of the two competing phases were confirmed by calculating the phonon spectra. Secondly, we discussed the elastic and electronic properties of two Li_4Ge phases. The results obtained here can enrich the Li-Ge phase diagram and may provide an important reference for the application of LIBs in practice. We believe that our study can further stimulate experimental and theoretical studies on alkali metal-IVA compounds.

2. Computational methods

The evolutionary algorithm USPEX²⁷⁻²⁹ in combined with the VASP package³⁰ is capable of predicting the stable structure of a compound under the specific chemical

composition. Here, the structure predictions were performed at 0 GPa, 5 GPa, and 10 GPa for Li₄Ge with the constraint that the total number of atoms in the unit cell is up to 20. In the evolutionary structural searching, a plane-wave basis set cutoff of 600 eV and a coarse k-point grid were used to perform the Brillouin zone integrations. The first generation of structures was created randomly with a population size of 120 structures. The succeeding generations were produced by variation operator heredity 40 %, lattice mutation 20 %, and permutation 20 %. The candidate structural relaxation was performed using density functional theory (DFT) within the generalized gradient approximation (GGA)³¹ as implemented in the VASP code.³⁰ The projector augmented wave (PAW) method was used to treat core electrons.³² The electron configurations 1s²2s¹ and 3d¹⁰4s²4p² are treated as valence states for Li and Ge, respectively. A higher Brillouin zone sampling of $2\pi \times 0.028 \text{ \AA}^{-1}$ and the plane-wave basis set cutoff of 600 eV were used, in order to ensure that the enthalpy calculations were converged within 1 meV/atom. Structural relaxation was stopped when the force generally acting on the atom was found to be less than 0.001 eV/Å. Phonon spectra calculations were conducted by finite displacement method as implemented in the PHONOPY code.^{33,34} The elastic constants were calculated based on linear response theory.³⁵ Using the obtained elastic constants C_{ij} , the bulk modulus B and shear modulus G were calculated using the Voight-Reuss-Hill (VRH) approximation.³⁶ Young's modulus E and Poisson's ratio ν can be calculated by formulae $E = \frac{9BG}{3B+G}$, $\nu = \frac{3B-2G}{2(3B+G)}$.

Results and discussions

3.1 Crystal structure

In our crystal structure search, we have found two competing structures (space group $P2_13$ and $R-3m$). The corresponding crystallographic information at ambient pressure condition is listed in Table 1. For the $P2_13$ phase, there are three different Wyckoff sites, Ge (4a), Li1 (12b) and Li2 (4a). Each Ge atom is six-fold coordinated by Li atoms

(three Li1 and three Li2), forming irregular octahedrons as shown in Figure 1a. The bond lengths are 2.60 Å for Li1-Ge and 2.66 Å for Li2-Ge, respectively. The octahedrons are connected by sharing Li2 atoms located at the vertices. For the hexagonal $R\text{-}3m$ phase, the (distorted) cubic hexahedron (where length of each side of the distorted cubes is either 2.96 Å or 3.25 Å) consisting of Li-sharing eight-fold GeLi_8 is similar with the structure of Li_4Si .²³ Ge atoms occupy the $3b$ sites. Three-fold coordinated Li1 atoms occupy the crystallographic $6c$ sites. Li2 atoms locating at $6c$ sites are only connected with one Ge atom. One can notice that a one-dimensional array of Li-Li-Li-Li-Ge runs along c -axis periodically, as shown in Figure 1b. In the GeLi_8 cube, each Li1 atom is connected with three neighboring Ge atoms from the adjacent cubes, while each Li2 atom is connected with one Ge atom within the cube. Thus, the formation of the structure can be interpreted based on the extended Zintl–Klemm principle where Ge atoms fulfill the “octet” by acquiring two electrons from six Li-atoms and two more electrons from other two Li-atoms, as expected. At zero pressure, the shortest Li-Li distance in $R\text{-}3m$ is 2.75 Å, which is shorter than 2.83 Å in $P2_13$. The shortest Li-Ge distance (2.70 Å) is longer than 2.66 Å in $R\text{-}3m$. The analogical structures of $R\text{-}3m$ Li_4Ge were proposed for Li_4Si ²³, and Li_4Sn ²⁴ in two recent computational studies, while the cubic phase is an entirely new structure which has not been reported in the literature to our knowledge.

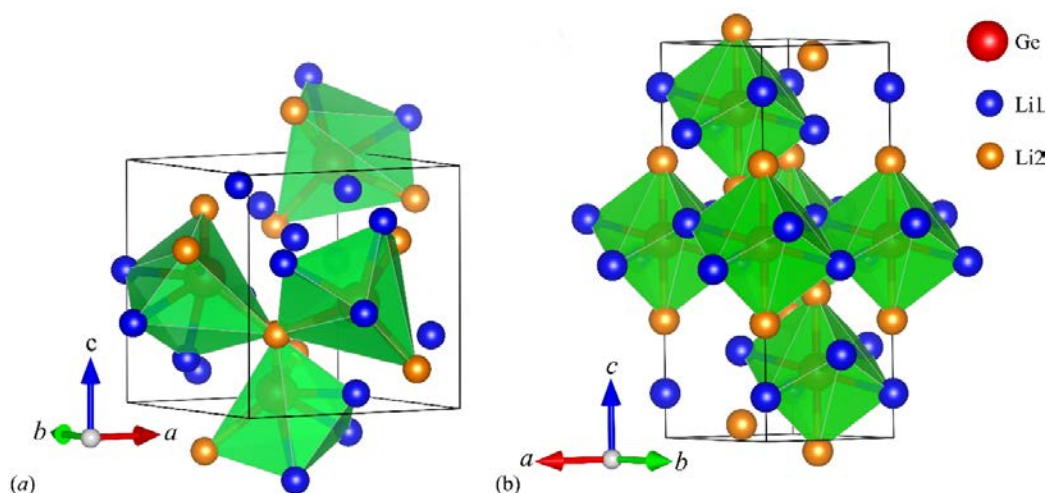


Figure 1. Crystal structures of Li_4Ge : (a) $P2_13$, (b) $R-3m$. Small green balls, small orange balls, and big red balls represent the Li1 atoms, Li2 atoms and Ge atoms, respectively.

Table 1. Lattice parameters and atomic positions of Li_4Ge at ambient pressure condition.

Space group	Density (g/cm^3)	Lattice parameters (\AA , deg)	Atomic fractional coordinate
$P2_13$	2.018	$a = b = c = 6.8441$ $\alpha = \beta = \gamma = 90.00$	Li1 $12b$ (0.9355, 0.1249, 0.2968) Li2 $4a$ (0.3127, 0.3127, 0.3127) Ge1 $4a$ (0.9498, 0.9498, 0.9498)
$R-3m$	2.141	$a = b = 4.5050$ $c = 13.2938$ $\alpha = \beta = 90$ $\gamma = 120$	Li1 $6c$ (0.0000, 0.0000, 0.1132) Li2 $6c$ (0.0000, 0.0000, 0.2997) Ge1 $3b$ (0.0000, 0.0000, 0.5000)

2. Phase transition

In order to determine the stability of two new Li_4Ge phases, we recalculated the convex hull diagram of Li-Ge at zero temperature and ambient pressure condition. As shown in Figure 2, the $\text{Li}_{17}\text{Ge}_4$, $\text{Li}_{15}\text{Ge}_4$, Li_8Ge_3 , $\text{Li}_{13}\text{Ge}_5$, Li_7Ge_3 , and LiGe phases are all thermodynamically stable with respect to dissociation into the elements, while Li_4Ge , $\text{Li}_{11}\text{Ge}_3$, Li_7Ge_2 , $\text{Li}_{13}\text{Ge}_4$, Li_5Ge_2 , Li_9Ge_4 , $\text{Li}_{11}\text{Ge}_6$, $\text{Li}_{12}\text{Ge}_7$ and $\text{Li}_7\text{Ge}_{12}$ are metastable ones theoretically. $P2_13$ - Li_4Ge is marginally stable. Its decomposition energy to the $\text{Li}_{17}\text{Ge}_4$ and $\text{Li}_{15}\text{Ge}_4$ is only 6 meV/atom, suggesting that the synthesis of $P2_13$ - Li_4Ge is highly possible. On the other hand, the $R-3m$ phase is slightly less favorable, which is 40 meV/f.u. higher in energy than $P2_13$. However, the relative phase stability with such small energy difference could be easily switched due to pressure. Therefore, we calculated the enthalpies of two competing phases as a function of pressure between 0

and 10 GPa. As shown in Figure 3(a), one can see that under the compression, the cubic $P2_13$ phase transforms to the rhombohedral hexagonal $R-3m$ at 2.0 GPa. Figure 3(b) shows the volume per chemical formula unit as a function of pressure for the two phases. It is obvious that the phase transition is accompanied by a sudden volume decrease (by 4.13 % at 2.0 GPa.), indicating that this is a first-order phase transition.

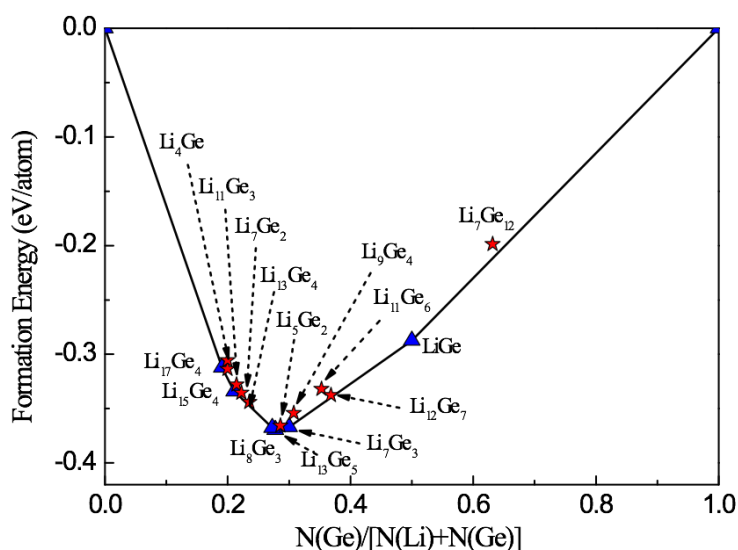


Figure 2. The calculated convex hull diagram of Li-Ge at 0 K and 0 GPa. The red pentacle means metastable phase, and blue triangle indicates stable one.

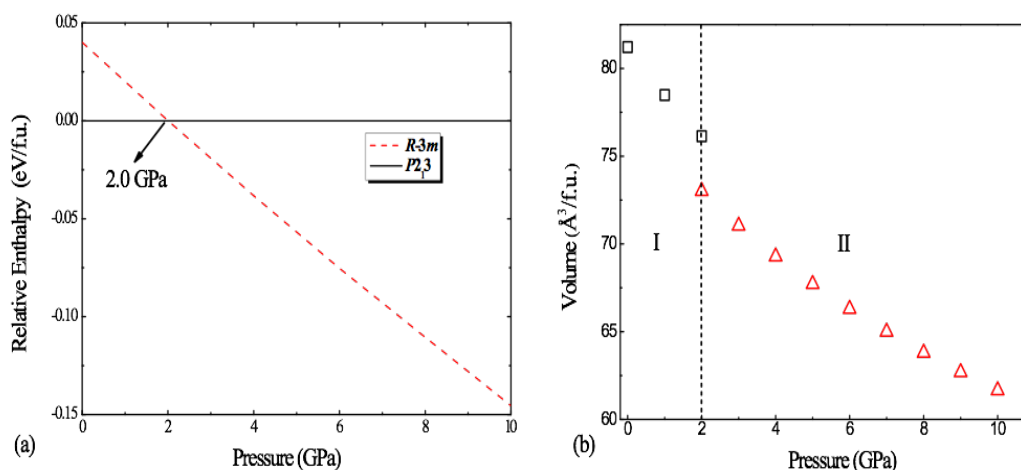


Figure 3. (a) Enthalpy difference versus pressure for two phases of Li_4Ge . (b) Volume versus pressure. Squares and triangles represent the I- $P2_13$ and II- $R-3m$, respectively.

3. Dynamical properties

To assessing the dynamical stability of Li_4Ge , we calculated the phonon spectra of $P2_13\text{-Li}_4\text{Ge}$ and $R-3m\text{-Li}_4\text{Ge}$. The phonon dispersion curves along the high-symmetry

direction and partial phonon density of states (PHDOS) were plotted in Figure 4(a) and Figure 4(b) for $P2_13$ -Li₄Ge and $R-3m$ -Li₄Ge, respectively. Both phonon dispersion curves show all positive frequencies in the entire Brillouin zone, indicating the dynamical stability. Thus they are likely to survive as long as the materials can be synthesized. Although two structures are different, their maximum optical branch frequencies are very similar (12.408 THz for the $P2_13$ phase and 12.71 THz for the $R-3m$ phase) at 0 GPa. From the PHDOS, one can conclude that the acoustic branches are mainly attributed to the vibrations from the Ge atoms (below about 5 THz), whereas higher-frequency optical branches are mainly from Li1 and Li2 atoms, which matches the fact that the Ge atoms are much heavier than the Li atoms.

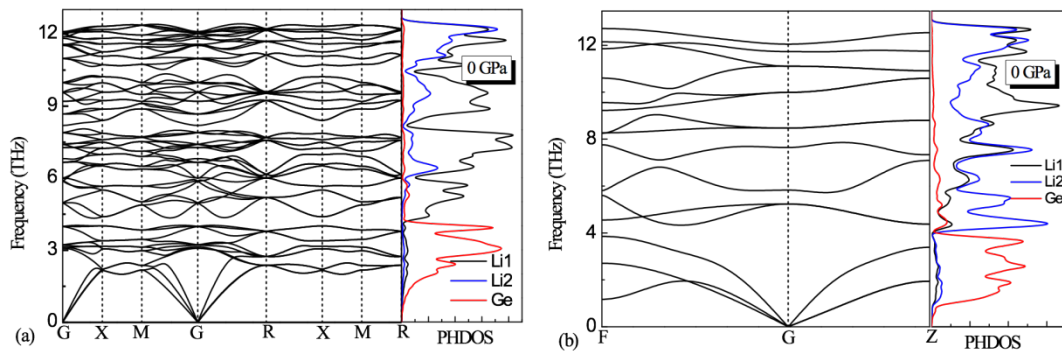


Figure 4. Phonon dispersion curves and partial atomic phonon density of states (PHDOS) of phonon spectrum of (a) $P2_13$ Li₄Ge and (b) $R-3m$ Li₄Ge at 0 GPa.

4. Elastic properties

It is well known that the elastic anisotropy of crystals is correlated with the mechanical behavior and the possibility to induce microcracks in the materials.³⁷ Hence, it is important to discuss the elastic anisotropy so as to understand the mechanical properties of Li₄Ge. In the case of cubic crystal system, Born-Huang stability criteria are well known: $C_{44} > 0$, $C_{11} - C_{12} > 0$ and $C_{11} + 2C_{12} > 0$.^{38, 39} There are six independent elastic constants for the rhombohedral structure (Laue class $-3m$), where the required mechanical stability criteria follows the inequalities $C_{11} > |C_{12}|$, $C_{44} > 0$, $C_{13}^2 < (C_{11} +$

C_{12}) and $C_{14}^2 < \frac{1}{2}C_{44}(C_{11} - C_{12}) \equiv C_{44}C_{66}$.^{38, 39} The calculated elastic constants C_{ij} are presented in Table 2. Clearly, the calculated elastic constants for $P2_13$ -Li₄Ge and $R-3m$ -Li₄Ge satisfy the Born-Huang criteria, suggesting that they are mechanically stable are well.

From the calculated elastic constants, one can derive a series of elastic properties such as the bulk modulus B , shear modulus G , Young's modulus E and Poisson's ratio ν based on the VRH approximation (see Table 2). Young's modulus is often used to provide a metric of stiffness of the material. The $P2_13$ phase and $R-3m$ phase have a Young's modulus of 46.9 GPa and 43.0 GPa at zero GPa, respectively. At the pressure of 2.0 GPa, the structure of $R-3m$ is getting stiffer. According to Pugh's criterion,⁴⁰ if the ν value of B/G is lower (higher) than 1.75, the material is brittle (ductile). The calculated values B/G indicated that $P2_13$ and $R-3m$ are both brittle. The universal anisotropic index A^U is defined as $A^U = 5 \frac{G_V}{G_R} + \frac{B_V}{B_R} - 6$.⁴¹ Zero value of A^U indicates the local isotropy. The deviation of this parameter from zero indicates the anisotropy of the crystalline structure. From Table 2, one can conclude that the $R-3m$ is more anisotropic than $P2_13$ at ambient pressure.

Table 2. The calculated elastic constants, bulk modulus B (GPa), shear modulus G (GPa), Young's modulus E (GPa), Poisson's ratio ν , and A^U for the $P2_13$ phase at 0 GPa and for $R-3m$ phase at 0 GPa and 2 GPa.

	P (GPa)	C_{11}	C_{44}	C_{12}	C_{33}	C_{13}	C_{14}	B	G	E	ν	B/G	A^U
$P2_13$	0	44.2	26.2	20.0	--	--	--	28.1	19.2	46.9	0.22	1.46	0.76
$R-3m$	0	82.3	7.8	9.4	78.1	-3.3	-11.7	27.8	17.3	43.0	0.24	1.60	11.62
$R-3m$	2	96.0	9.47	12.7	93.8	-2.6	-12.7	33.3	20.8	51.6	0.24	1.60	9.11

3.5 Electronic properties

The calculated electronic band structure along the high symmetry directions in the BZ and the corresponding PDOS at 0 GPa are shown in Figure 5. Our electronic structure

calculations show that the $P2_13$ phase is a semiconductor with a narrow band gap of 0.117 eV. On the other hand, $R-3m$ Li_4Ge is metallic, in which three bands cross the Fermi level along the F-G direction. In both $P2_13$ - Li_4Ge and $R-3m$ - Li_4Ge , Ge- p states dominate the whole valance bands while Li- p states have minor contribution.

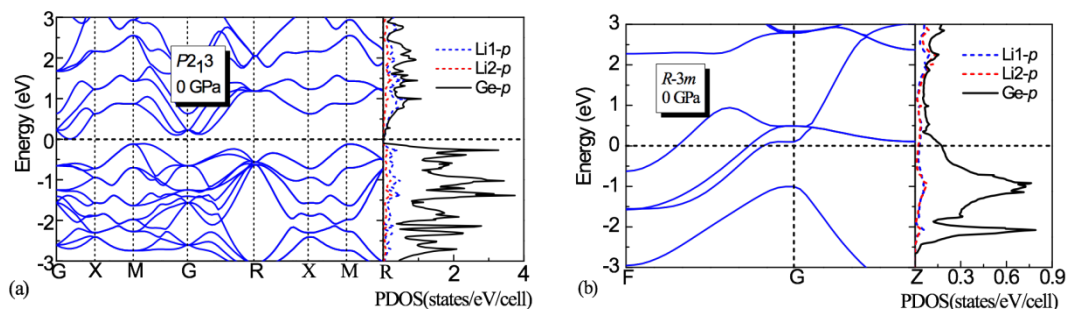


Figure 5. The electronic band structure and projected density of states (PDOS) at 0 GPa for (a) $P2_13$ Li_4Ge and (b) $R-3m$ Li_4Ge .

4 Conclusions

In summary, two structures were proposed for Li_4Ge by using the evolutionary algorithm structure searching. The $P2_13$ phase was found to be stable below 2.0 GPa, while the $R-3m$ phase is stable above 2.0 GPa. The calculated phonon spectra and elastic constants confirmed their dynamical and mechanical stabilities. Elastic calculations suggest that the $P2_13$ structure is brittle, while the $R-3m$ structure is ductile. The $R-3m$ structure is more anisotropic than the $P2_13$ structure at ambient pressure. The electronic structure shows that $P2_13$ phase is a semiconductor, while $R-3m$ phase is a metal. We believe our findings do not only enrich the phase diagram of Li-Ge system, but also are beneficial to the design of new anode materials of LIBs.

Acknowledgements

Work at JNSU is support from the NSFC (Grant No. 11674131) and the Priority Academic Program Development of Jiangsu Higher Education Institutions (PAPD). Work at UNLV is supported by the National Nuclear Security Administration under the Stewardship Science Academic Alliances program through DOE Cooperative Agreement DE-NA0001982. We thank the use of computing resources from XSEDE and High Performance Computing Center at JNSU.

- a) qiang.zhu@unlv.edu
- b) ylli@jsnu.edu.cn

Reference

1. D. Liu, Z. J. Liu, X. Li, W. Xie, Q. Wang, Q. Liu, Y. Fu, D. He, *Small*, 2017, **13**, 1236-1247.
2. M. Armand, J. M. Tarascon, *Nature*, 2008, **451**, 652-657.
3. A. G. Morachevskii, *Russ. J. Appl. Chem.*, 2017, **89**, 1561-1572.
4. H. Tian, F. Xin, X. Wang, W. He, W. Han, *Journal of Materiomics*, 2015, **1**, 153-169.
5. C.M. Park, J.H. Kim, H. Kim, H.J. Sohn, *Chem. Soc. Rev.*, 2010, **39**, 3115-3141.
6. C.Y. Chou, H. Kim, G. S. Hwang, *J. Phys. Chem. C*, 2011, **115**, 20018-20026.
7. X. H. Liu, S. Huang, S. T. Picraux, J. Li, T. Zhu, J. Y. Huang, *Nano letters.*, 2011, **11**, 3991-3997.
8. T. Song, H. Cheng, H. Choi, J. H. Lee, H. Han, D. H. Lee, D. S. Yoo, M. S. Kwon, J. M. Choi, S. G. Doo, H. Chang, J. Xiao, Y. Huang, W. I. Park, Y. C. Chuang, H. Kim, J. A. Rogers, and U. Paik, *ACS Nano*, 2012, **6**, 303-309.
9. Y. Yu, C. Yue, S. Sun, W. Lin, H. Su, B. Xu, J. Li, S. Wu, J. Li, J. Kang, *ACS Appl. Mater. Interfaces*, 2014, **6**, 5884-5890.
10. J. Sangster, A. D. J. Pelton, *J. Phase Equilib.*, 1997, **18**, 289-294.
11. G. R. Goward, N. J. Taylor, D. C. S. Souza, L. Nazar, *J. Alloys Compd.*, 2001, **329**, 82-91.
12. A. J. Morris, C. P. Grey, C. J. Pickard, *Phys. Rev. B*, 2014, **90**, 054111.
13. E. M. Pell, *J. Phys. Chem. Solid State Phys.*, 1957, **3**, 74-76.
14. G. I. Oleksiv, *Probl. Rozvitka Prirodn. i. Tochn. Nauk.*, 1964, 76-77.
15. P. I. Federov and V. A. Molochka, *Izv. Akad. Nauk. SSSR, Neorg. Mater*, 1966, **2**, 1870-1871.
16. A. Grüttner, R. Nesper, H. G. von Schnering, *Acta Crystallogr. A*, 1981, **37**, C-161.
17. A. Grüttner, PhD thesis, University of Stuttgart, 1982
18. E. L. Gladyshevskii, G. I. Oleksiv, and P. I. Kripyakevich, *Sov. Phy. Crystallogr*, 1964, **9**, 269.
19. E. I. Gladyshevskii, G. I. Oleksiv and P. I. Kripyakevich, *Kristallografiya*, 1964, **9**, 338-341.
20. Q. Johnson, G. S. Smith and D. Wood, *Acta Crystallogr.*, 1965, **18**, 131-132.
21. R. Nesper, *Prog. Solid State Chem.*, 1990, **20**, 1-45.
22. M. Zeilinger, T. F. Fässler, *Dalton Trans.*, 2014, **43**, 14959-70.
23. S. T. Zhang, Y. C. Wang, G. C. Yang, Y. M. Ma, *ACS Appl. Mater. Interfaces*, 2016, **8**, 16761-16767.
24. R. Sen, P. Johari, *ACS Appl. Mater. Interfaces*, 2017, **9**, 40197-40206.
25. C.M. Hao, Y. Li, H. M. Huang, Y. L. Li, *J. Chem. Phys.*, 2018, **148**, 204706.
26. Y. Lin, T. A. Strobel, R. E. Cohen, *Phys. Rev. B: Condens. Matter*, 2015, **92**, 214106
27. A. O. Lyakhov, A. R. Oganov, H. T. Stokes, Q. Zhu, *Comput. Phys. Commun.*, 2013, **184**, 1172-1182.
28. A. R. Oganov, C. W. Glass, *J. Chem. Phys.*, 2006, **124**, 244704-244715.
29. A. R. Oganov, A. O. Lyakhov, M. Valle, *Acc. Chem. Res.*, 2011, **44**, 227-237.
30. W. Dong, G. Kresse, J. Furthmüller, J. Hafner, *Phys. Rev. B: Condens. Matter*, 1996, **54**, 2157-2166
31. J. P. Perdew, K. Burke, and M. Ernzerhof, *Phys. Rev. Lett.*, 1996, **77**, 3865-3868.
32. P. E. Blöchl, *Phys. Rev. B*, 1994, **50**, 17953-17979.
33. K. Parlinski, Z. Q. Li, Y. Kawazoe, *Phys. Rev. Lett.*, 1997, **78**, 4063-4066.
34. A. D. Becke, K. E. Edgecombe, *J. Chem. Phys.*, 1990, **92**, 5397.
35. J. A. Pople, P. W. G. Gill, B.G. Johnson, *Chem. Phys. Lett.*, 1992, **199**, 557-560.
36. R. Hill, *Proc. Phys. Soc. A.*, 1952, **65**, 349-354.
37. X. X. Sun, Y. L. Li, G. H. Zhong, H. P. Lü, Z. Zeng, *Phys. Rev. B: Condens. Matter*, 2012, **407**, 735-739.
38. F. Mouhat, F. X. Coudert, *Phys. Rev. B*, 2014, **90**, 224104.
39. M. Born and K. Huang, *Dynamics Theory of Crystal Lattices* (Oxford University Press, Oxford, UK, 1954).
40. S. F. Pugh, XCII. *Philos. Mag.*, 1954, **45**, 823-843.
41. S. I. Ranganathan, M. Ostojca-Starzewski, *Phys. Rev. Lett.*, 2008, **101**, 055504.